Structured ultrasound microscopy

Jovana Janjic,[1] Pieter Kruizinga,[1] Pim van der Meulen,[2] Geert Springeling,[3] Frits Mastik,[1] Geert Leus,[2] Johan G. Bosch,[1] Antonius F. W. van der Steen,[1,4] and Gijs van Soest[1]
[1]*Thoraxcenter, Biomedical Engineering, Erasmus Medical Center, Rotterdam 3000 CA, The Netherlands*
[2]*Faculty of Electrical Engineering, Mathematics and Computer Science–Micro Electronics, Delft University of Technology, 2628 CD Delft, The Netherlands*
[3]*Department of Experimental Medical Instruments, Erasmus Medical Center, 3015 CN Rotterdam, The Netherlands*
[4]*Faculty of Applied Science-Imaging Physics, Delft University of Technology, 2600 AA Delft, The Netherlands*

(Received 24 February 2018; accepted 23 April 2018; published online 18 June 2018)

We present a form of acoustic microscopy, called Structured Ultrasound Microscopy (SUM). It creates a volumetric image by recording reflected echoes of ultrasound waves with a structured phase front using a moving single-element transducer and computational reconstruction. *A priori* knowledge of the acoustic field produced by the single element allows us to relate the received echoes to a 3D scatter map within the acoustic beam itself, leading to an isotropic resolution at all depths. An aberration mask in front of the acoustic element imposes the phase structure, broadening the beam and breaking the spatial coherence between different voxels at equal acoustic propagation delay, increasing the uniqueness of the reconstruction. By translating the transducer across the 3D volume, we synthetically enlarge the imaging aperture by using multiple overlapping and spatially sparsely sampled measurements to solve for the entire image. In this paper, we explain the SUM technique and demonstrate microscopic imaging at 20 MHz of a $2.3 \times 2.3 \times 1.2$ mm object in water, with an isotropic resolution below 100 μm. The proposed approach allows for wide-field 3D imaging at isotropic microscopic resolution using a small unfocused ultrasound sensor and multiple spatially sparsely sampled measurements. This technique may find applications in many other fields where space is constrained, device simplicity is desired, and wide-field isotropic high-resolution imaging is required. https://doi.org/10.1063/1.5026863

High-resolution wide-field ultrasound microscopy is of great interest for different applications ranging from non-destructive testing of small electronic components[1] to tissue microscopy[2–5] and intravascular imaging.[6–8] Scanning acoustic microscopy (SAM) enables high resolution imaging using a high frequency, tightly focused ultrasound transducer. Image data are acquired by scanning the transducer or the object under study in two dimensions while acquiring pulse-echo A-lines.[9] The imaged volume is obtained by mapping the backscattered echoes to a 3D image grid. The lateral resolution depends on the numerical aperture and varies over the depth, with the highest resolution achieved at the focal distance; the axial resolution is proportional to the acoustic bandwidth. The depth-varying, anisotropic resolution, the large number of sampling points needed for full 3D coverage, and the complexity of manufacturing high-frequency focused transducers limit the utility of SAM in many practical applications. In this work, we propose Structured Ultrasound Microscopy (SUM), a wide-field imaging technique with isotropic high resolution. SUM exploits the spatial *a priori* information of a structured ultrasound beam and achieves volumetric imaging with a set of measurements spatially sampled on a sparse grid.

Computational imaging has attracted broad interest recently, as it has enabled simultaneous wide field-of-view and high image resolution, often realized in compact, simple imaging systems. It forms an image by solving an inverse mathematical problem, using *a priori* knowledge of the imaging system. Some technologies developed in the past decade include synthetic aperture microscopy,[10] Fourier ptychographic microscopy,[11,12] and lensless imaging.[13,14] Synthetic aperture techniques were developed for radar to improve resolution by moving the recording system (e.g., mounted on an airplane) and combining multiple overlapping signals.[15] Image resolution is determined by the compounded aperture, which is wider than the instrument aperture.

Lensless optical imaging systems achieve high-resolution, wide-field imaging[13,14] by replacing the lens with an aperture mask that modulates the illumination and encodes high-frequency spatial information in the available aperture. The use of aperture masks to encode spatial information has also been considered in ultrasonic imaging.[16–18] The mask scrambles the incident sound field, destroying the spatial coherence, similar to speckle formation. The resulting fine-scale structure in the beam enables enhanced resolution imaging, as in imaging through scattering media.[19]

Recently, we showed that knowledge of the complex ultrasound field created by the aperture mask allows 3D imaging using only one sensor.[18] SUM is based on that concept: scanning acoustic microscopy with phase-encoded insonification. It employs a 3D-printed phase mask to encode 3D spatial information in the acoustic delay and inverse modeling of the imaging system to achieve wide-field high-resolution

volumetric imaging. In this way, we can overcome the limitations of SAM, where dense sampling is required and high resolution is achieved only in the focal region of the transducer. We also investigate synthetic aperture microscopy with computational reconstruction, without an aperture mask (which we call Scanning Reconstructed Ultrasound Microscopy; RUM), to independently assess the benefits of computational reconstruction and beam scrambling.

The mathematical model for computational reconstruction[18] describes the pulse-echo signal for each voxel in the imaging region for a given ultrasound field (with and without the mask), scanned over a sparsely sampled grid. We denote this as the system matrix $\boldsymbol{H}$. Volumetric imaging is achieved by inversion of this model. We denote the measurement vector $\boldsymbol{u}$, and we assume that it is linearly related to the image $\boldsymbol{v}$ through the following equation:

$$\boldsymbol{u} = \boldsymbol{H}\boldsymbol{v} + \boldsymbol{n}, \tag{1}$$

where $\boldsymbol{n}$ is the additive noise. The image $\boldsymbol{v}$, containing the scattering amplitude per voxel, can be computed with linear inversion methods, such as regularized least squares inversion using the LSQR algorithm.[18]

As shown in Fig. 1, a custom-built unfocused single-element piezoelectric ultrasound transducer (20 MHz, 1 mm diameter) was mounted on a rigid tube and clamped on a motorized positioning stage (Newport Corporation, CA, USA). The coding mask was fabricated using stereolithography (Nanoscribe, Karlsruhe, Germany). It consisted of square pillars (80 μm sides; comparable to the wavelength in water) with random heights (between 40 and 320 μm). This mask affects local delays of up to several wavelengths to the wave field. The speed of sound in the printed resin is 2500–2700 m/s.[20] The mask was slightly larger than the transducer to facilitate assembly. After mounting the mask on the transducer, we covered it with silicone to improve the mechanical stability. The transducer was excited with a 10 ns, 60 V unipolar pulse (Avtech Electrosystems Ltd, USA). After amplification by 40 dB (MITEQ, USA) and bandpass filtering (10–30 MHz, 5th order Butterworth), the received echo was digitized at 400 MS/s and 12-bit resolution (Agilent Technologies, USA). A custom-built expander/limiter electrically separated the transmitted and the received signal path. All the measurements were performed in a water tank at room temperature.

The spatiotemporal impulse response of the two transducers (with and without mask) was mapped by first scanning a plane perpendicular to the propagation direction, using a 75 μm needle hydrophone (Precision Acoustics, UK). The spatiotemporal impulses were acquired on a 4×4 mm grid with a dense 30 μm spacing at a distance of 900 μm from the transducer. Using the angular spectrum of the measurements in this plane, we then computed the forward field impulse responses of the voxels in any parallel plane.[21] Finally, assuming reciprocity, we autoconvolved the forward field impulse-response of each pixel to get their scattered echo signals. The resulting traces are then used to populate the system matrix $\boldsymbol{H}$. All the signal processing is implemented in Matlab 2016b (The MathWorks, MA, USA). To reduce the computational complexity, we chose a sparse Fourier-domain representation of each voxel signal (band-limited between 15 and 25 MHz).

The ultrasound field transmitted by the single element transducer without mask exhibits a mild natural focus at approximately 3 mm (Fig. 2). When the mask is placed in front of the transducer, the scrambled phase of the ultrasound field leads to a complex interference pattern. This interference pattern reduces the similarity between nearby voxels

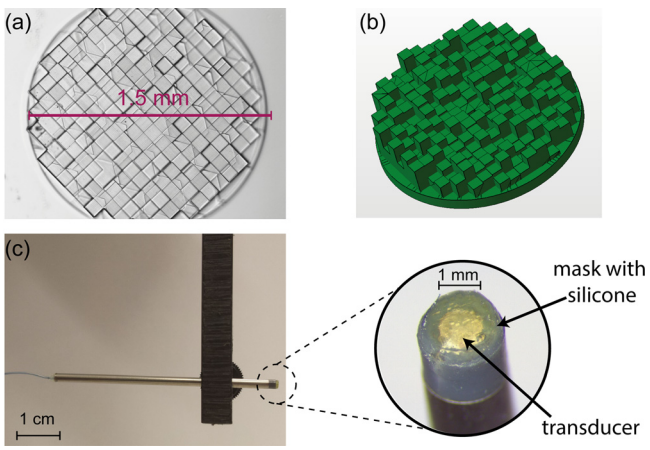

FIG. 1. (a) Top view of the aperture mask imaged with a microscope, (b) schematic drawing of the aperture mask, and (c) transducer with the mask mounted on the translation stage with close up on the transducer with mask.

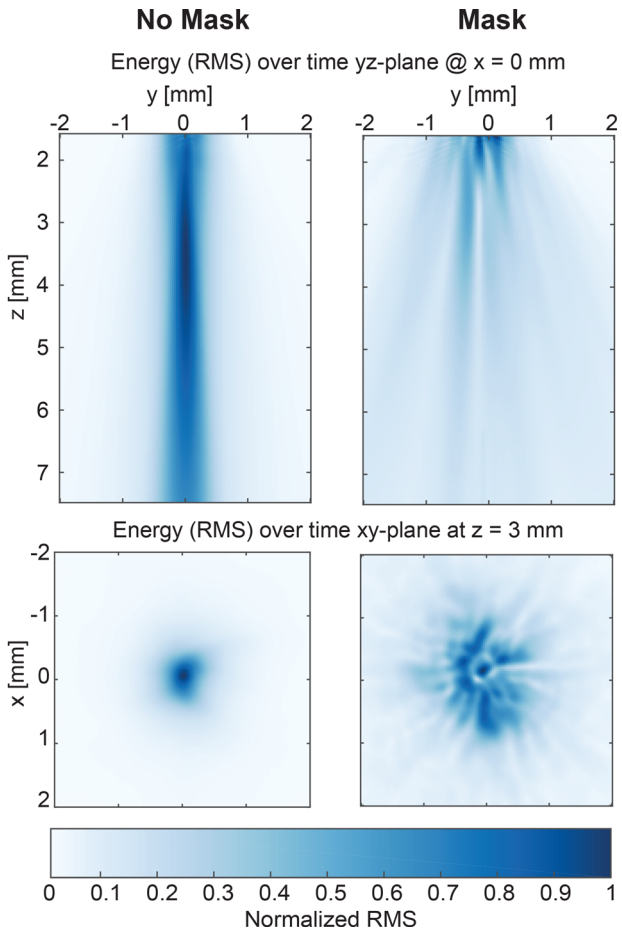

FIG. 2. Ultrasound field transmitted from the sensor without (left column) and with the aperture mask (right column). The propagating medium is water.

resulting in pulse-echo signals that are highly uncorrelated [Fig. 3(a)] and increases the field-of-view [Fig. 3(b)]. For full volumetric imaging without (RUM) and with mask (SUM), we acquire measurements at different locations, similar to SAM. However, in SAM, the width of the focal region determines the lateral resolution in the plane perpendicular to the ultrasound propagation axis (the *x, y* plane). This means that high lateral resolution is achieved by a narrow beam and a dense spatial sampling. In both RUM and SUM, we resolve the *x* and *y* components in the beam by exploiting the ultrasound spatial information in the imaging plane, without the need for a tightly focused beam. In SUM, the mask produces a broader beam, and so, fewer measurements are required to cover the same area compared to SAM and RUM. Even with sparse spatial sampling, there is a significant overlap between the beams, further reducing the similarity of the voxels [Fig. 3(c)].

We compute the absolute correlations between the pulse-echo signals in $\boldsymbol{H}$ that correspond to the imaging voxel in a single plane for a given measurement pattern. Figure 4(a) shows the correlations between the pulse-echo signal of one voxel (scatterer) and the pulse-echo signals of all other voxels in the analysis plane, with a scanning step size of 300 μm in both *x* and *y* directions for both the cases without (RUM) and with (SUM) the mask. The correlation is always high for neighboring voxels, making it difficult to resolve two different scatterers, and decreases as one moves further away from the scatterer. We observe that with the mask, high image resolution is achieved by fast decorrelation for increasing distances from the scatterer, at the cost of a slight increase in background clutter. We show the absolute correlation for the increasing voxel-to-scatterer distance, averaged in the scan plane, in Fig. 4(b).

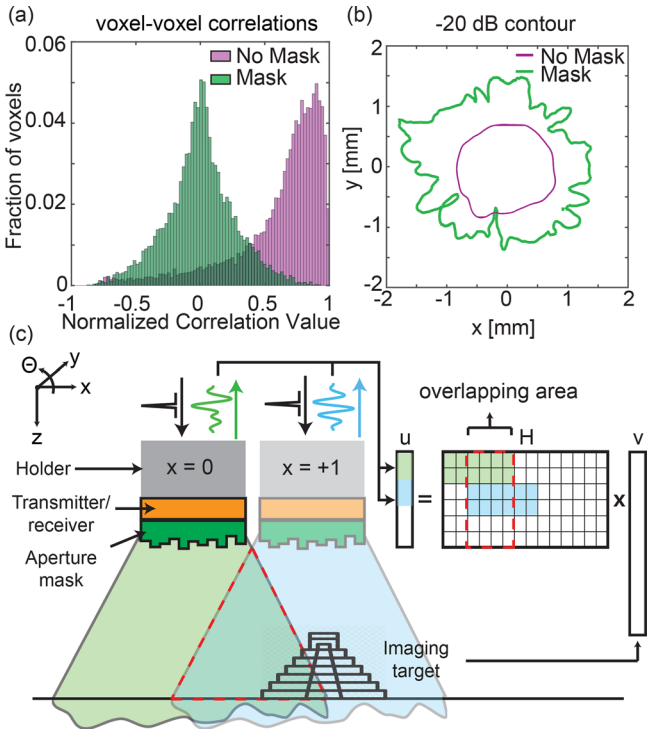

FIG. 3. (a) Histogram of voxel-to-voxel correlations between all the voxels in one *x, y* plane and (b) −20 dB contour plot of the ultrasound beam in the *x, y*-plane for both the cases without and with the mask; (c) schematic of the imaging procedure.[18]

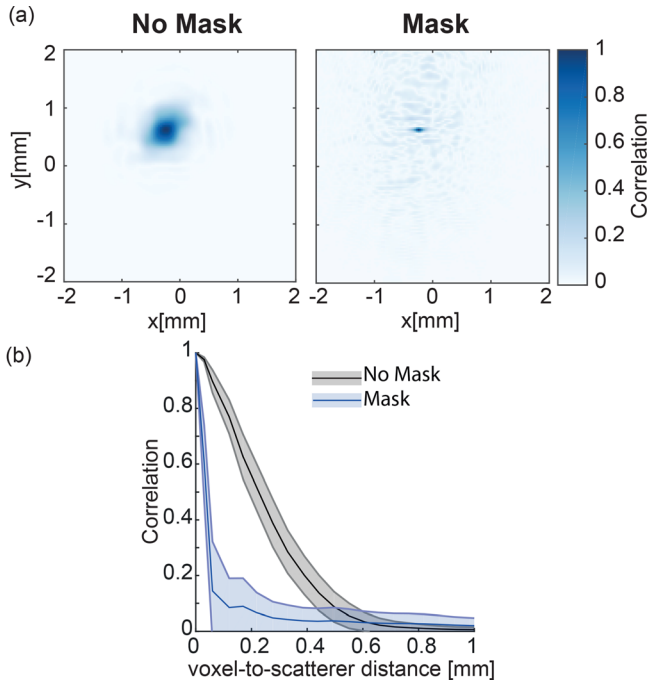

FIG. 4. Analysis of the in-plane correlation. (a) Correlation of one reference voxel in the plane (located at x = −0.5 and y = 0.5 mm) for the case without and with the mask, using a scan step size of 300 μm; (b) average of all the voxel correlations versus voxel-to-scatterer distance (mean ± standard deviation).

We experimentally demonstrate computational ultrasound for high-resolution wide-field imaging of a 3D-printed object (Miicraft) with dimensions of $2.3 \times 2.3 \times 1.2$ mm [Fig. 5(a)]. The object was glued on rubber and submerged in water at 3 mm from the transducer. Reconstruction of the image by mapping the pulse-echo signal envelope to a 3D imaging grid by scanning the region of interest (4×4 mm) with a 30 μm step (SAM-like imaging) results in a poor image [Fig. 5(b)]. Next, we perform a computational reconstruction without and with mask, using a randomly selected subset containing 40% of the densely sampled measurements and using the LSQR algorithm [Figs. 5(c)–5(e)].

Both RUM and SUM result in highly improved resolution. Even without the mask (RUM), the small imperfections in the transducer introduce spatial heterogeneity in the beam allowing reconstruction of the object with recognizable features down to ∼150 μm. When the mask is used (SUM), the image fidelity is further improved, with the smallest structures (80 μm) resolved [Figs. 5(d) and 5(e)] (Multimedia view). This result also demonstrates that exploiting the spatial information of the ultrasound field results in isotropic resolution. Increased resolution and field-of-view are obtained by encoding 3D spatial information on echo delays using an aperture mask. The gain in resolution comes at the expense of a reduction in signal to noise ratio (SNR) by approximately 10 dB. We attribute this SNR loss to the acoustic energy being emitted into a larger volume and to the impedance mismatch of the transducer-mask-water interfaces.

Improvement in the SNR can be achieved by optimizing mask materials and geometry. In this work, we used a mask that was 3D printed, hence limiting the material choice to resins suitable for the specific printer. Beside the choice of the mask material, accurate optimization of the mask

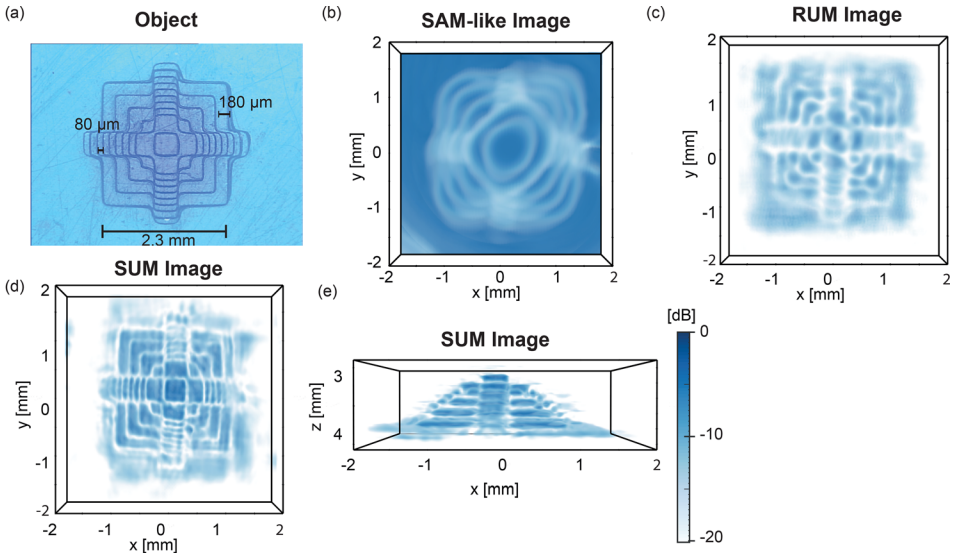

FIG. 5. (a) Top view of the 3D object imaged with a microscope; reconstructed image using (b) conventional SAM-like imaging, (c) RUM, and (d) and (e) SUM. Multimedia view: https://doi.org/10.1063/1.5026863.1

geometry should be performed.[22] By optimizing the mask geometry, more spatial diversity could be introduced, such that unique signals are associated with each voxel, leading to a model matrix $\boldsymbol{H}$ with highly uncorrelated columns. This will enable recovery of the 3D image with microscopic resolution using fewer measurements. Moreover, if the $\boldsymbol{H}$ matrix is characterized with high accuracy, better image reconstruction can be achieved. The hydrophone used in our measurements had a 75 μm sensor, equal to the wavelength of the 20 MHz acoustic waves in water. Subwavelength sampling of the ultrasound field will lead to a more complete characterization of $\boldsymbol{H}$, improving image resolution.

The imaging method that we propose here could also be applied to irregular scanning patterns if the transducer position is known at every scan. Compact tracking techniques, such as optics-based systems,[23,24] may enable the implementation of SUM in minimally invasive medical imaging devices. Catheter-based imaging has demonstrated to be a powerful tool for guidance of cardiac and vascular interventions,[25] but present-day imaging catheters do not achieve comprehensive, high-resolution microscopy. SUM hardware is small, cheap, and simple, and it is compatible with miniature disposable devices.

In conclusion, SUM is a form of acoustic microscopy that enables wide-field isotropic high-resolution imaging with a simple unfocused ultrasound transducer and a cheap coding mask. This technique may find applications in many fields where space is constrained and wide-field high-resolution imaging is required.

This research was partially supported by the Dutch Technology Foundation STW (Grant Nos. 12710 and 14926), which is part of the Netherlands Organization for Scientific Research (NWO) and which is partly funded by the Ministry of Economic Affairs.

We are grateful to Jeroen Mesman at Leiden University for fabricating the acoustic mask.

[1]M. Y. Mehr, A. Bahrami, H. Fischer, S. Gielen, R. Corbeij, W. D. v. Driel, and G. Q. Zhang, "An overview of scanning acoustic microscope, a reliable method for non-destructive failure analysis of microelectronic components," in *EuroSimE* (2015), pp. 1–4.

[2]A. F. W. Van Der Steen, C. L. De Korte, and J. M. Thijssen, "Ultrasonic spectroscopy of the porcine eye lens," Ultrasound Med. Biol. **20**, 967–974 (1994).

[3]C. L. De Korte, A. F. W. van der Steen, and J. M. Thijssen, "Acoustic velocity and attenuation of eye tissues at 20 MHz," Ultrasound Med. Biol. **20**, 471–480 (1994).

[4]F. S. Foster, C. J. Pavlin, K. A. Harasiewicz, D. A. Christopher, and D. H. Turnbull, "Advances in ultrasound biomicroscopy," Ultrasound Med. Biol. **26**, 1–27 (2000).

[5]K. Kumagai, H. Koike, R. Nagaoka, S. Sakai, K. Kobayashi, and Y. Saijo, "High-resolution ultrasound imaging of human skin *in vivo* by using three-dimensional ultrasound microscopy," Ultrasound Med. Biol. **38**, 1833–1838 (2012).

[6]C. Chandrana, J. Talman, T. Pan, S. Roy, and A. Fleischman, "Design and analysis of MEMS based PVDF ultrasonic transducers for vascular imaging," Sensors **10**, 8740–8750 (2010).

[7]F. Guo, C. Liu, Y. Yang, L. Sun, B. Yang, Y. Chen, and J. Dai, "Development of focused IVUS transducer using PMN-PT single crystal," in *2014 IEEE International Ultrasonics Symposium (IUS)* (2014), pp. 97–100.

[8]P. D. Corl, "Focused rotational IVUS transducer using single crystal composite material," Google Patents WO2014100690A1, 2014.

[9]R. A. Lemons and C. F. Quate, "Acoustic microscopy: Biomedical applications," Science **188**, 905–911 (1975).

[10]T. Turpin, L. Gesell, J. Lapides, and C. Price, "Theory of the synthetic aperture microscope," Proc. SPIE **2566**, 230–240 (1995).

[11]G. Zheng, R. Horstmeyer, and C. Yang, "Wide-field, high-resolution Fourier ptychographic microscopy," Nat. Photonics **7**, 739–745 (2013).

[12]X. Ou, R. Horstmeyer, C. Yang, and G. Zheng, "Quantitative phase imaging via Fourier ptychographic microscopy," Opt. Lett. **38**, 4845–4848 (2013).

[13]J. K. Adams, V. Boominathan, B. W. Avants, D. G. Vercosa, F. Ye, R. G. Baraniuk, J. T. Robinson, and A. Veeraraghavan, "Single-frame 3D fluorescence microscopy with ultraminiature lensless FlatScope," Sci. Adv. **3**, e1701548 (2017).

[14]N. Antipa, G. Kuo, R. Heckel, B. Mildenhall, E. Bostan, R. Ng, and L. Waller, "DiffuserCam: Lensless single-exposure 3D imaging," Optica **5**, 1–9 (2018).

[15]K. Tomiyasu, "Tutorial review of synthetic-aperture radar (Sar) with applications to imaging of ocean surface," Proc. IEEE **66**, 563–583 (1978).

[16]K. Melde, A. G. Mark, T. Qiu, and P. Fischer, "Holograms for acoustics," Nature **537**, 518–522 (2016).

[17]M. D. Brown, D. I. Nikitichev, B. E. Treeby, and B. T. Cox, "Generating arbitrary ultrasound fields with tailored optoacoustic surface profiles," Appl. Phys. Lett. **110**, 094102 (2017).

[18]P. Kruizinga, P. van der Meulen, A. Fedjajevs, F. Mastik, G. Springeling, N. de Jong, J. G. Bosch, and G. Leus, "Compressive 3D ultrasound imaging using a single sensor," Sci. Adv. **3**, e1701423 (2017).

[19]I. M. Vellekoop and A. P. Mosk, "Focusing coherent light through opaque strongly scattering media," Opt. Lett. **32**, 2309–2311 (2007).

[20]See https://www.ndeed.org/GeneralResources/MaterialProperties/UT/ut_matlprop_plastics.htm for NDT Resource Center.
[21]P. R. Stepanishen and K. C. Benjamin, "Forward and backward projection of acoustic fields using FFT methods," J. Acoust. Soc. Am. **71**, 803–812 (1982).
[22]P. Van der Meulen, P. Kruizinga, J. G. Bosch, and G. Leus, "Spatial compression in ultrasound imaging," in Fifty-First Asilomar Conference on Signals, Systems and Computers, IEEE, 2017.
[23]M. E. Froggatt, J. W. Klein, D. K. Gifford, and S. T. Kreger, "Optical position and/or shape sensing," U.S. patent 8,773,650 (08 July 2014).
[24]R. G. Duncan, M. E. Froggatt, S. T. Kreger, R. J. Seeley, D. K. Gifford, A. K. Sang, and M. S. Wolfe, "High-accuracy fiber-optic shape sensing," Proc. SPIE **6530**, 65301S (2007).
[25]G. S. Mintz and G. Guagliumi, "Intravascular imaging in coronary artery disease," Lancet **390**, 793–809 (2017).